ACS APPLIED ENGINEERING MATERIALS

pubs.acs.org/acsaenm

Article

Preparation and Characterization of a Disilylated Naphthalenediimide Molecular Crystal: Perspectives for Organosilica Mesoporous Materials

Renan Gabriel de Assis, Marcos de Oliveira Junior, Márcia Tsuyama Escote, Carlos Basílio Pinheiro, José Javier Sáez Acuña, Fabio Furlan Ferreira, Luana Sucupira Pedroza, Sergio Brochsztain,* and Thiago Branquinho de Queiroz*

Cite This: *ACS Appl. Eng. Mater.* 2024, 2, 1976−1986

Read Online

ACCESS | Metrics & More | Article Recommendations | Supporting Information

ABSTRACT: Naphthalenetetracarboxylic diimides (NDIs) are efficient electron acceptors due to their high electron affinity. They are applied in heterogeneous catalysis and organic electronics. In this work, we report, for the first time, the synthesis of *N*,*N*′-bis[3-(triethoxysilyl)propyl]-1,4,5,8-naphthalenediimide (NDI-silane) as a molecular crystal obtained from recrystallization in petroleum ether. The compound is stable in air conditions and chloroform solution. Its crystal structure was determined by single-crystal X-ray diffraction. We have characterized the intermolecular dispersive interactions by density functional theory calculations, indicating that the stability of the crystal in air conditions is related to dispersive interactions. Furthermore, we characterize the optical and photoelectrical properties of thin NDI-silane films, demonstrating photoinduced conductivity over a wide range of temperatures (10−300 K). Remarkably, a venture of NDI-based organosilica can be obtained from stable NDI-silane crystals, prominent materials in organoelectronics and photocatalysis. As a proof of concept, we prepare mesoporous organosilicas with 100% NDI-silane using the ionic liquid 1-butyl-3-methylimidazolium tetrafluoroborate as a templating and sol−gel catalytic agent. These materials show a well-formed organosilica network, presenting only T_3 and T_2 Si species, as probed by solid-state ^{29}Si NMR. As a result, the mesoporous materials are considerably more resistant to thermal degradation than the crystals, being stable up to 450 °C. According to N_2 adsorption isotherms and transmission electron microscopy images, they demonstrate microporous and mesoporous structures associated with narrow slitlike pores.

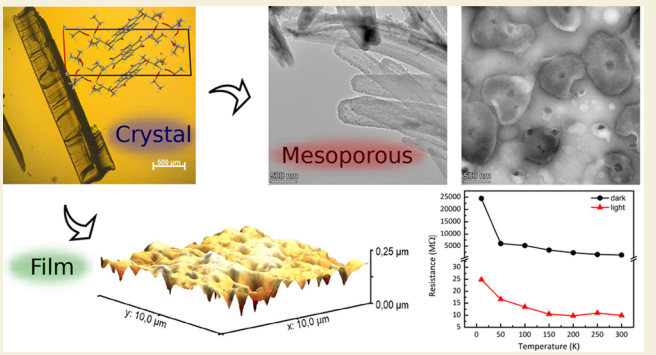

KEYWORDS: *naphthalenediimide, organic electronics, sol−gel synthesis, mesoporous organosilica, photoconductivity properties*

1. INTRODUCTION

Naphthalenetetracarboxylic diimides (NDIs) are electron-deficient aromatic systems that have been proposed as backbones or skeletons for electron acceptor applications due to their relatively high electron affinity, as well as their thermal and ambient air stability.[1−3] They are chemically flexible and can be easily synthesized from naphthalenetetracarboxylic dianhydride (NTCA) with primary amines, which allows for the synthesis of NDI derivatives with a wide range of amine substituents.[1,3] In particular, one can functionalize NDI with oxysilane groups to allow sol−gel chemistry in functional materials.[4−6] The two-step reduction of the NDIs gives rise to relatively stable anion radicals and dianions. The reduction can be accomplished by chemical,[7−9] electrochemical,[10] or photochemical[11] routes. Since the first report of the high electron mobility displayed by some NDI derivatives,[12] they have attracted increasing attention as n-type organic semiconductors for organic electronics.[13−15] In addition, they are prone to π-stack and promote intermolecular electron transfer, enhancing charge-transport efficiency.[2,16] The NDIs have also been employed as organic field-effect transistors,[16−18] light-emitting diodes,[19] electrochromic and photochromic materials,[20−22] photocatalyst agents,[23] lithium-ion batteries,[24] and gas storage.[7]

In this work, we report for the first time the preparation and characterization of *N*,*N*′-bis[3-(triethoxysilyl)propyl]-1,4,5,8-naphthalenediimide (NDI-silane) as a molecular crystal (see the structure in Figure 1). Its composition and stability in solution were characterized by NMR spectroscopy. The crystal

Received: May 23, 2024
Revised: June 25, 2024
Accepted: June 27, 2024
Published: July 8, 2024

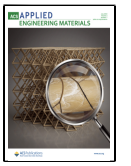

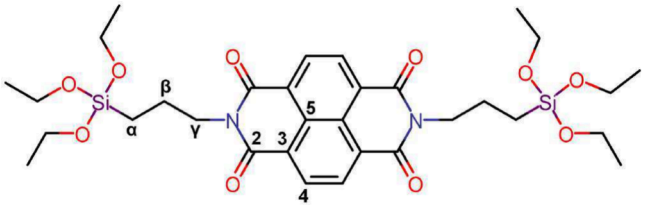

Figure 1. 2D representation of the NDI-silane structure.

structure was obtained from single-crystal X-ray diffraction (SCXRD) and confirmed by the Laue patterns of electron diffraction of single crystals in transmission electron microscopy (TEM). The formation and stability of the NDI-silane crystal are understood by the intermolecular interaction between the NDI rings and siloxyl groups.

The syntheses of analogous pyromellitimide (PMI) and perylenediimidediimide (PDI) derivatives, namely, *N*,*N*′-bis[3-(triethoxysilyl)propyl]pyromellitimide[25−28] and *N*,*N*′-bis[3-(triethoxysilyl)propyl]-3,4,9,10-perylenediimidediimide,[29−33] have already been reported. In a previous paper, we reported the extraction of NDI-silane by reacting NTCA over (3-aminopropyl)triethoxysilane, then precipitating a solid in petroleum ether, and finally extracting the pure compound in acetone.[6] We prepared mesoporous organosilicas SBA-15-NDI and demonstrated their photocatalytic activity in the photodegradation of sulfadiazine.[6] It was also possible to prepare photochromic thin films.[34] However, it is very challenging to obtain mesoporous organosilicas containing high amounts of the organic precursor without compromising their structure from such solutions. In the previous report, we could prepare an organosilica that preserves the SBA-15 structure by mixing only up to 16% by weight of NDI-silane with 84% of tetraethylorthosilicate.[6]

The synthesis of NDI-silane as a stable and widely soluble molecular crystal opens possibilities for the preparation of new organosilicas with controlled inorganic-to-organic ratios, molecular packing, and morphology by taking advantage of sol−gel chemistry in the ethoxysilane group. This permits the preparation of a rigid NDI-modified silica network, aiming for high electron transport simultaneously with increased durability, which is crucial in many applications. We present here the preparation of a NDI-silane thin film and mesoporous organosilica containing 100% NDI-silane using the ionic liquid (IL) 1-butyl-3methylimidazolium tetrafluoroborate as a templating and sol−gel catalytic agent. The thin film was characterized by its optical and electrooptical properties in combination with time-dependent density functional theory (TD-DFT) calculations. The mesoporous materials were characterized by solid-state NMR, thermogravimetric analysis (TGA), N_2 adsorption isotherms, and TEM.

2. METHODS

2.1. Synthesis of a NDI-silane Crystal

For the preparation, 6 mL (26 mmol) of (3-aminopropyl)-triethoxysilane (APTES, Sigma-Aldrich) was heated to 130 °C in an oil bath. Then 1.62 g (6 mmol) of 1,4,5,8-naphthalenetetracarboxylic dianhydride (NTCA, Sigma-Aldrich) was added in small portions for about 5 min, resulting in a clear reddish solution. APTES acts as both a reagent and a solvent in this process. The mixture was allowed to cool and poured into 100 mL of petroleum ether, resulting in instantaneous precipitation. The crystallization was centrifuged at 10000 rpm for 10 min, resulting in two phases: supernatant and pellets. The supernatant, presenting an orange color, was collected in a beaker and stored at −18 °C for 24 h when orange crystals precipitate. The crystals were collected, washed with 10 mL of cold petroleum ether (Synth), and vacuum-dried for 3 h at ambient temperature, yielding about 860 mg of NDI-silane crystals (21% yield), yet impure, with the remaining APTES.

The resulting 860 mg of crystals were subjected to recrystallization to purify them. They were dissolved in 120 mL of a 1:1 (v/v) solution of petroleum ether with ethyl ether (Synth), heated to the boiling temperature, cooled, filtered, and stored until they form new pure crystals. The storage was made in two different conditions. In the first condition, the solution was stored at −18 °C for 24 h when orange microcrystals were formed. In the second condition, the solution was stored at ambient temperature for 4 days until it formed single crystals. Figure S1 shows digital photographs and optical microscopy images of NDI-silane microcrystals formed at −18 °C and single crystals at ambient temperature.[35]

The crystals were collected and washed with 10 mL of a petroleum ether/ethyl ether solution and dried under vacuum for 4 h, obtaining around 410 mg of stable and pure NDI-silane crystals (10% yield).

2.2. Preparation of Thin Films by Spin Coating and Characterization of Morphology

NDI-silane thin films were spin-coated from tetrahydrofuran (THF) solutions in cleaned glass substrates. For optimization of the film thicknesses, different rotation speeds, droplet volumes, and solution concentrations were evaluated. Regarding the concentration, we started with solutions of 20 and 30 g L^{-1}. The droplet volume was varied at 100 and 150 μL, and the rotation speed was at 700, 850, 1000, and 1250 rpm for 30 s. The samples were subjected to thermal treatment from 30 to 80 °C with a heating rate of 10 °C/h. The best parameters were based on the target thickness (≈300 nm) and homogeneity, as obtained by the surface profiles of a Tencor P-7 profiler and by atomic force microscopy (AFM) with an Agilent 5500 series instrument at room temperature. Scanning electron microscopy (SEM) was obtained with a JEOL JSM-6010LA scanning electron microscope using a secondary electron imaging detector with an acceleration voltage of 10 kV.

2.3. Preparation of Mesoporous Silica

The protocols for preparing mesoporous organosilica were based on ref 36. In the first step, 40 mg of benzoic acid was solubilized in 3.15 mL of ethanol (Synth, P.A.). Then, 0.75 mL of a 0.1 M HCl solution and 55, 29, and 14 μL of the IL 1-butyl-3methylimidazolium tetrafluoroborate (99.9%, Sigma-Aldrich) were added to this vessel, according to NDI-silane/IL molar ratios of 1:2, 2:1, and 4:1, respectively (see the molar quantities in Table 1). In another vessel,

Table 1. Molar Quantities of the Precursors for the Preparation of Organosilicas

sample	NDI:IL molar ratio	benzoic acid (mmol)	NDI-silane (mmol)	IL (mmol)
NDI-silica A	1:2	0.54	0.47	0.96
NDI-silica B	2:1	0.35	0.31	0.16
NDI-silica C	4:1	0.35	0.31	0.08

200 mg of NDI-silane crystal was solubilized in 3.15 mL of acetone. Then, the second solution was added dropwise to the first, and the mixture was poured into a Petri dish. The solution solidified between 15 min and 3 h, and the solid was allowed to dry at room temperature for 1 week, followed by drying for 24 h at 60 °C and 72 h at 80 °C. Finally, the IL was removed via Soxhlet extraction in acetonitrile for 2 days, followed by drying of the resulting powder for 24 h at 80 °C. We did not observe traces of the IL in the ^{1}H or ^{13}C NMR spectra of the mesoporous materials.

2.4. Powder X-ray Diffraction (PXRD)

The NDI-silane crystals were crushed before the PXRD measurement. Data were collected in transmission geometry on a STADI-P

https://doi.org/10.1021/acsaenm.4c00341
ACS Appl. Eng. Mater. 2024, 2, 1976−1986

diffractometer (Stoe, Darmstadt, Germany) with Cu Kα_1 radiation (λ = 1.54056 Å) selected by a curved Ge(111) crystal, with a tube voltage of 40 kV and a current of 40 mA. A Mythen 1K detector (Dectris, Baden, Switzerland) recorded the pattern from 2.000° to 111.935° (2θ) in steps of 0.015° and a counting time of 100 s at each 1.05°. The indexed PXRD pattern is displayed in Figure S2.[35]

2.5. Single-Crystal X-ray Diffraction (SCXRD)

SCXRD experiments were conducted using an Oxford Gemini diffractometer with Cu Kα radiation at around 200 K. X-ray diffraction data integration and scaling of the reflection intensities were performed with the *CrysAlisPro 1.171.42.68a* suite. The final unit cell parameters were based on fitting all measured reflection positions. Analytical numeric absorption correction using a multifaceted crystal model was based on expressions derived by Clark and Reid.[37] Empirical absorption correction was employed using spherical harmonics, implemented in the *CrysAlisPro SCALE3 ABSPACK* scaling algorithm.

The program *XPREP*[38] was used for the space group identification and final data reduction, and the structures were solved using the *SHELXT* program,[39] implemented in *WinGX*.[40] The positions of all but the hydrogen atoms could be unambiguously assigned on consecutive difference Fourier maps.

Refinements were performed using *SHELXL*[41] based on F^2 through the full-matrix least-squares routine. The hydrogen atoms of all methyl, methylene, and aromatic groups were added to the structure in idealized positions and further refined according to the riding model [C−H = 0.97 Å; U_{iso}(H) = 1.2U_{eq}(C)]. All except hydrogen atoms were refined with anisotropic atomic displacement parameters. The crystal data, data collection, temperature, and structure refinement details are summarized in Table S1. The CIF file has already been deposited with the CCDC under deposition number 2351484.

2.6. TEM and Electron Diffraction

The structural investigation of the samples was also carried out using a high-resolution transmission electron microscope (Thermo Fischer Talos F200X-G2) operating at a 200 kV accelerating voltage using a field-emission gun. The diffraction patterns were obtained by the selected-area electron diffraction technique using a physical aperture of 200 nm.

2.7. Liquid-State NMR

Liquid-state ^{1}H, ^{13}C, and ^{29}Si NMR spectra were measured with a Varian VNMRS 500 MHz spectrometer operating at the resonance frequencies 99.3 MHz (^{29}Si) and 125.7 MHz (^{13}C). The measurements were done by 45° single pulse (SP), ^{1}H COSY, and ^{1}H{^{13}C} HSQC at a temperature of 27 °C in static samples. The parameters for the ^{1}H and ^{13}C NMR spectra were standard, around 4 μs for the pulse length and 1 s for the recycle delay and acquisition time. For ^{29}Si NMR, a 6−8 s recycle delay was needed for full relaxation (as observed by an inversion−recovery T_1 measurements). The COSY's parameters were 0.5 s for acquisition time, 1 s for relaxation delay, mixing delay of 20 ms, acquiring 512 increments in the indirect dimension until 0.1 s evolution time, with 4 transients collected (in the direct dimension). The HSQC parameters were 0.5 s for the acquisition time and 1 s for the relaxation delay, acquiring 128 increments in the indirect dimension until 0.006 s evolution time, with 16 transients collected (in the direct dimension). The spectra are displayed in Figures S3−S8.[35]

2.8. Solid-State NMR Spectroscopy

Solid-state ^{29}Si NMR experiments were conducted with the same Varian VNMRS 500 MHz spectrometer at a magic angle spinning (MAS) of 15 kHz (SP-MAS) at ambient temperature (around 23 °C) using the tppm ^{1}H decoupling pulse sequence.[42] Typical acquisition parameters were a ^{1}H-π/2 pulse length of 2.5 μs and a ^{29}Si-π/2 of 3.5 μs, with a relaxation delay of 100 s. ^{1}H and ^{13}C NMR experiments were performed with a 600 MHz Avance Neo Bruker spectrometer with typical π/2 pulse lengths of 1.2 and 2.0 μs for ^{1}H and ^{13}C, respectively. ^{1}H double quantum−single quantum (DQ−SQ) experiments were performed under 60.8 kHz MAS using an R14$^5_4$ symmetry-based homonuclear recoupling scheme with no homonuclear decoupling during DQ evolution.[43] ^{1}H{^{13}C} cross-polarization (CP) and heteronuclear correlation (HETCOR) spectra were measured at 60 kHz MAS with ^{1}H detection, using a double-CP pulse sequence,[44] with a contact time of 2 ms. The ^{1}H{^{13}C} HETCOR spectrum of the NDI-silane crystal is displayed in the paper and that of NDI-silica A in Figure S9,[35] for completeness. Chemical shifts are reported relative to tetramethylsilane at 0 ppm for all isotopes, using α-glycine as a secondary reference, ^{13}C[δ(C═O)] = 176.5 ppm and ^{1}H[δ(NH_3)] = 8.5 ppm.[45,46] Talc was used as a secondary reference for ^{29}Si with an isotropic chemical shift at −98.1 ppm.

2.9. Optical Spectroscopy

The UV−vis absorption spectra of a 10^{-4} M toluene solution and thin film were obtained with a Varian Cary 50 spectrophotometer at room temperature. The emission and excitation spectra were obtained with a Shimadzu RF-6000 spectrofluorimeter with an incident beam at an angle of ≈30° and a detector at ≈60° concerning the normal vector for the thin film.

2.10. Photoconductivity Characterization of the NDI-silane Thin Film

For the electrical conductivity, two gold electrodes were deposited 0.35(1) mm apart on the film's surface by thermal evaporation at 10^{-4} Pa using a gold mass of 13 mg. The distance between the electrodes was measured in an optical microscope. This geometry permits reproducible measurements to be performed over various temperatures. Temperature dependence was done on an ARS closed-circuit cryostat system coupled to a 331 Lakeshore temperature controller. The measurements were performed with a Keithley 2400 C sourcemeter with a current of 1−10 μA over a temperature range of 10−300 K in the dark and under the incidence of a λ = 405 nm laser with a power of 1000 W at a fixed distance of 5 cm. The beam laser area has 3 mm^2; thus, the light power per area applied was 333 W/mm.

2.11. TGA and N_2 Isotherm Adsorption

TGA was performed with a TA Instruments Q500 analyzer, recorded at a heating rate of 10 °C/min from 30 to 800 °C in a nitrogen atmosphere.

The N_2 adsorption isotherms were obtained with a Quantachrome model Nova 2200e. Initially, the samples were degassed for 24 h at 110 °C to remove water and impurities. Next, N_2 adsorption isotherms were measured over 60 points until saturation. The surface area of the mesopores were calculated using the Brunauer−Emmett−Teller (BET) method.[47] In addition, the pore-size distribution was determined by the Barrett−Joyner−Halenda (BJH) method at the desorption points of the isotherms.[48]

2.12. DFT and TD-DFT Calculations

We performed DFT calculations under boundary periodic conditions to relax the crystal structure, calculate the binding energies appropriately for finite systems, obtain the binding energies of the NDI pairs, and interpret the optical properties of the thin film.

2.12.1. Calculations with Periodic Boundary Conditions. The DFT calculations were based on a localized orbital description of the Kohn−Sham wave functions as implemented in the *Siesta* code[49] and considering a nonlocal van der Waals (vdW) xc-functional, as proposed by Berland and Hyldgaard.[50] The core electrons were described by norm-conserving pseudopotentials in the Troullier−Martins form,[51] and the valence electrons were described using a double-ζ-polarized (DZP) basis set of numerical atomic orbitals.

2.12.2. Calculations for Finite Systems. The starting geometry of the NDI-silane as a single molecule was taken from the naphthalenediimide crystal structure (CCDC 945184) [and replaced the dimethylamine for (triethoxysilyl)propyl]. The starting geometry of the H-cluster system, emulating a viable cluster geometry in the thin film, was obtained by approximating the two molecules at plane-to-plane distances smaller than equilibrium distances (typically 3.4 Å). After geometry optimization of this H-dimer, they were replicated and

https://doi.org/10.1021/acsaenm.4c00341
ACS Appl. Eng. Mater. 2024, 2, 1976−1986

twisted in order to approximate one (triethoxysilyl)propyl site to the naphthalenediimide ring. These geometries were obtained from DFT geometry optimizations using the M06-2X functional[52] with the 6-31G(d,p) basis set. The binding energies of the NDI-silane molecular pairs obtained from the crystalographic data + DFT relaxed structures (section 2.12.1) were calculated using the same M06-2X functional with the 6-311G++(d,p) basis set, with the counterpoise correction to the basis set superposition error as proposed by Boys and Bernardi.[53] These DFT approximations have been shown to accurately reproduce the intermolecular distances and binding energies of parental molecular systems.[54]

Calculations of the ionization energies and excitation spectra were performed with the range separated hybrid (RSH) functional ωPBE,[55] composed of PBE_x (exchange) at short range and nonlocal Fock-like exact exchange (EXX) at long range, with PBE_c (correlation) at all ranges, also with the 6-31G(d,p) basis set. The range separation parameter (ω) was determined for each system following the established tuning procedure[56] of choosing ω such that the difference between the first ionization energies (ionization potential, IP, and electron affinity, EA) and the HOMO eigenvalues is minimized (ϵ_{HOMO}). This optimally tuned RSH (OT-RSH) functional approach has been shown to reproduce reliably localized and charge-transfer excited states.[57,58] Excitation spectra were obtained from linear response TD-DFT using the OT-RSH functional. The calculations described above were performed using the *Q-Chem* software.[59] All isosurface densities were plotted using the *Molden*[60] and *VMD*[61] plotting packages with a density factor of 0.01.

3. RESULTS

3.1. NDI-silane in Solution

In order to verify the purity of the compound, we characterized the compound in $CDCl_3$ by liquid-state NMR. The as-synthesized compound shows only peaks attributed to NDI-silane (for the ^1H and ^{13}C NMR spectra, see Figures S3–S8).[35] All correlations observed in the COSY and HSQC experiments led to the peak assignments as displayed in the Supporting Information[35] (note that the NMR shifts in solution are slightly different from the solid state in the NDI-silane crystal). Most remarkably, from the $^1H\{^{13}C\}$ HSQC experiment, we note that the peak at 130.9 ppm belongs to the protonated aromatic carbon atoms and the peaks at 126.6 and 126.7 ppm belong to the quaternary carbon atoms of the naphthalenediimide.[35] The ^{29}Si NMR spectrum has a single peak at −46.21 ppm (see below), similar to MPS-silane [3-(trimethoxysilyl)propyl methacrylate], observed at −43.16 ppm, and APTES, observed at −44.4 ppm,[62] indicating the presence of the ethoxysilane group without hydrolysis of the compound.

To test the stability of the compound in solution, the NMR tube was kept at ambient conditions for about 3 months and weekly; after solvent evaporation, the compound was diluted again in $CDCl_3$ and measured. For up to 8–9 weeks after synthesis, the compound was intact, and after 10 weeks, there were additional peaks, most remarkably at 0.90 ppm, accounting for about 15% compared to the CH_2 at 0.76 ppm (Table S2).[35] The same conclusions can be taken from the ^{13}C NMR spectra, with a peak at 29.7 ppm appearing in the 10th week (not shown).

3.2. NDI-silane Molecular Crystal

Figure 2a shows an optical microscopy image of a single crystal, Figure 2b shows a 2 × 2 × 2 supercell structure projecting along the *b* axis, as obtained by SCXRD, and Figure 2c shows the pair of nonequivalent NDI-silane molecules in the unit cell. The triclinic $P\bar{1}$ space group was confirmed by the

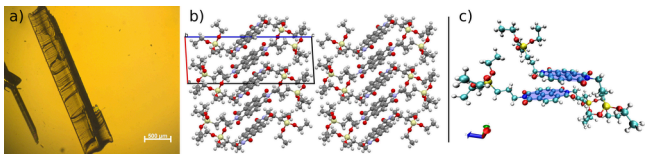

Figure 2. (a) Image of a single crystal taken with an optical microscope. (b) 2 × 2 × 2 supercell plot along the *b* axis of the NDI-silane crystal structure as determined by single-crystal DRX. (c) Structural detail of the π-stacked nonequivalent NDI-silane molecules. Blue circles are superposed in the NDI rings to emphasize their twisted orientation.

PXRD pattern (Figure S2)[35] and electron diffraction, with a unit cell of a = 8.4856(2) Å b = 8.9180(2) Å, and c = 23.0198(6) Å and α = 89.157(2)°, β = 86.667(2)°, and γ = 85.5892(2)°. Figure S10a shows the usual bright-field electrograph in TEM, and Figure S10b shows a high-angle annular-dark-field (HAADF) image by the scanning TEM technique[35] indicating the homogeneity of the crystals on a micrometric scale. Parts c–h of Figure S10[35] show six diffraction patterns for different crystallographic orientations, with their respective zone axes indexed.

The stability of the compound in air conditions is relatively unusual for organosilica compounds because the siloxyl groups are prone to hydrolysis in the presence of water. This property can be related to the intermolecular interactions in the crystal structure, which we discuss by simplifying them into molecular pairs. The unit cell has two nonequivalent π-stacked naphthalenediimide rings separated by about 3.5 Å that are twisted by a dihedral angle of 37° (Figure 2c). These molecules have a binding energy of 99.7 kJ/mol (1.03 eV), which is quite high compared to similar systems that are considered highly coupled. For comparison, Kumar et al. investigated the charge-transfer performance of several combinations of π-stacked donor–acceptor systems and found distinctive results for the pyrene–NDI pair.[63] Its good charge-transfer performance was correlated to a high association constant that was reasoned based on a frontier orbital congruence between the molecular units.[63] Its optimal interplanar distance is about 3.35 Å, and the binding energy is about 18 kcal/mol (0.19 eV).[54] Thus, this is the "piling up" interaction responsible for the stability of the compound along the *a* axis. Figure 3 shows a slice in the *c*-axis direction with three "lined-up" NDI-silane molecules and a "twisted" one. The lined-up molecules β and δ show a dispersive interaction between the siloxyl groups, with a binding energy of 21.4 kJ/mol (0.22 eV). This is the interaction responsible for the stability of the structure along the *c* axis. Finally, the lined-up molecule δ and the twisted molecule γ have their siloxyl groups dispersively interacting with a binding energy of 25.7 kJ/mol (0.27 eV). This interaction is responsible for the stability of the structure along the *b* axis.

We have also characterized the solid-state NMR features of the compound, which brings additional information. Figure 4 shows the solid-state ^{13}C CP-MAS NMR spectrum of the NDI-silane crystal and respective peak attributions in Table 2 (see the discussion on the mesoporous materials in section 3.4). The ^{13}C CP-MAS NMR spectrum for the NDI-silane crystal with 2 ms contact time is similar to the one in $CDCl_3$ (Figure S3),[35] except for an expected line broadening. Table 2 summarizes the ^{13}C and ^1H NMR peak assignments based on the liquid-state NMR and $^1H-^1H$ SQ-DQ and $^{13}C-^1H$ CP-

https://doi.org/10.1021/acsaenm.4c00341
ACS Appl. Eng. Mater. 2024, 2, 1976–1986

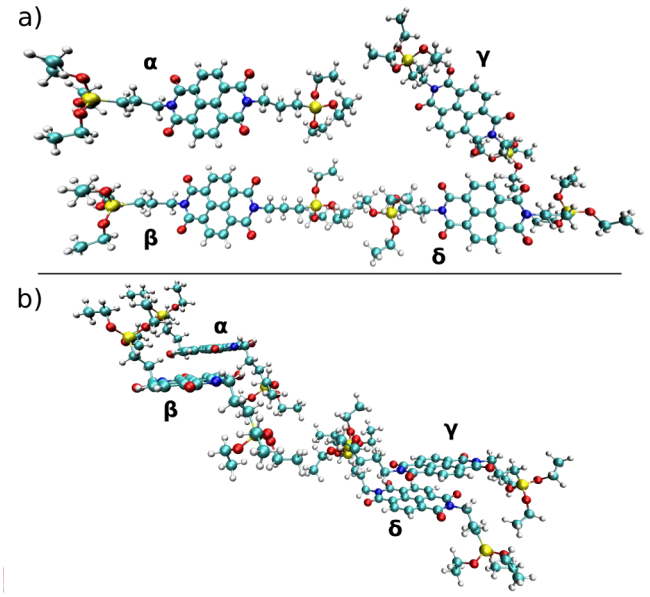

Figure 3. (a) Top projection (approximately along the *a* axis) and (b) side projection (approximately along the *b* axis) of a *b*-axis direction slice of the NDI-silane crystal structure. Molecules α, β, and γ are described as "lined-up" molecules, and molecule γ is described as a "twisted" molecule.

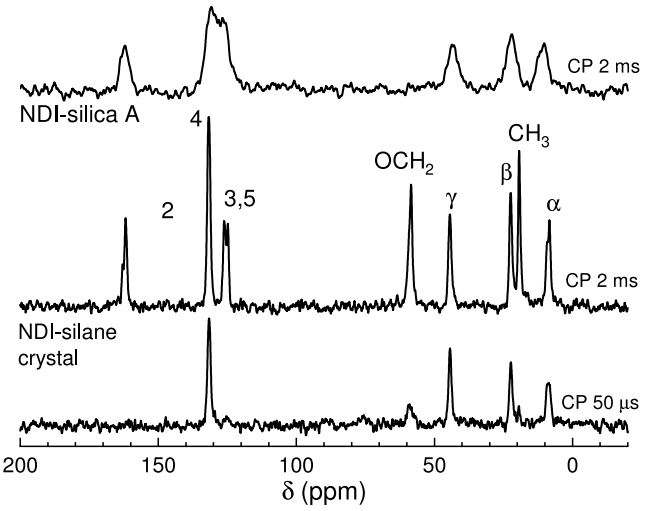

Figure 4. ^{13}C CP-MAS NMR spectra of the NDI-silane crystal and NDI-silica A. For the crystalline sample, a spectrum acquired using a short CP contact time of 50 μs is also shown.

Table 2. ^{13}C and ^{1}H NMR Assigned Peaks of the NDI-silane Crystal

assignment	^{13}C (±0.5 ppm)	^{1}H (±0.1 ppm)
C_α	8.5	0.8
C_β	22.6	2.0
C_γ	44.6	3.4
CH_3	19.6	1.3
OCH_2	59.3	3.8
C_2	161.8	
C_3, C_5	126.3/124.8	
C_4	131.8	8.5, 7.8

HETCOR correlations (discussed below). Note, however, that there is a split at 7.8 and 8.5 ppm for ^{1}H at the C_4 position, otherwise observed as one peak at 8.76 ppm in the liquid state. This is related to the nonequivalent molecules in the NDI-silane crystal structure, also noticeable in the ^{29}Si NMR (see below).

An additional CP-MAS experiment with a short contact time (50 μs) was performed, providing spectral editing (Figure 4, bottom). In this experiment, the signal for a nonprotonated or highly mobile carbon species is suppressed. A comparison of the spectra obtained for long contact and short contact times allows us confirm the previous attribution based on the $^{1}H\{^{13}C\}$ HSQC experiment. The peaks at 125.6 ppm are absent in the short-contact spectrum, while the opposite holds for the peak at 131.5 ppm. Notably, the ethyl groups are also lacking in the spectrum acquired with a short contact time, demonstrating that they are mobile species in the crystal structure.

The $^{1}H\{^{13}C\}$ HETCOR spectrum acquired with fast MAS (60 kHz) and proton detection for the NDI-silane crystal is shown in Figure 5. The experiment was carried out using a

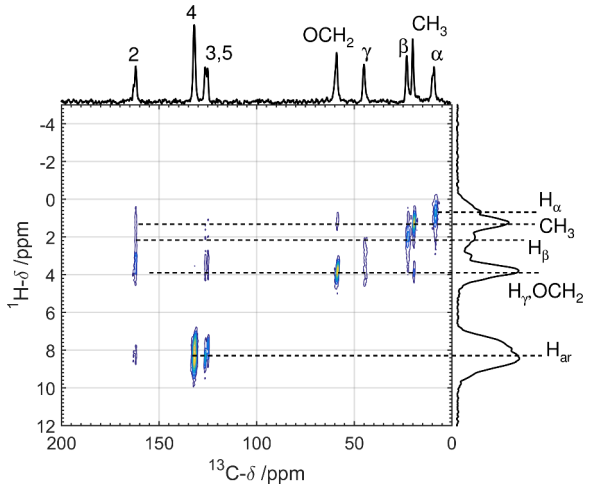

Figure 5. $^{1}H\{^{13}C\}$ HETCOR spectra of the NDI-silane crystal. The spectra were measured at 60 kHz MAS and a contact time of 2 ms. For simplicity, the projection in the ^{13}C dimension is the CP-MAS spectrum. Peak attributions are provided in Table 2.

relatively long contact time, 2 ms, in order to probe the H−C spatial proximity through the $^{1}H-^{13}C$ heteronuclear dipolar coupling. The spectrum shows the expected correlation peaks based on the molecular structure (Figure 1). ^{1}H species in the CH_2 (and CH_3) groups show chemical shifts in the range from 0.8 ppm (H_α) to 3.5 ppm (H_γ), while aromatic protons resonate at 7.8−8.5 ppm. Most interestingly, the $^{1}H\{^{13}C\}$ HETCOR spectrum shows a correlation between quaternary aromatic carbons 3 and 5 and the ethyl protons in the OCH_2 groups, indicating the spatial proximity of 5−6 Å between some of these sites for the nonequivalent molecules in the unit cell, as noted in the crystal structure.

Figure 6 shows a ^{1}H DQ-SQ NMR correlation spectrum for the NDI-silane crystal. As expected, double coherence is observed among the aromatic protons, OCH_2 and CH_3. It is also observed between the OCH_2−CH_3, OCH_2−aromatic, and CH_3−aromatic protons (off-diagonal terms).

Finally, the ^{29}Si NMR spectrum of the NDI-silane crystal shows two peaks at −45.1 and −46.6 ppm with 54% and 46% contributions, respectively, corresponding to the ethoxysilane group, as observed in the liquid-state ^{29}Si NMR (Figure 7).

https://doi.org/10.1021/acsaenm.4c00341
ACS Appl. Eng. Mater. 2024, 2, 1976−1986

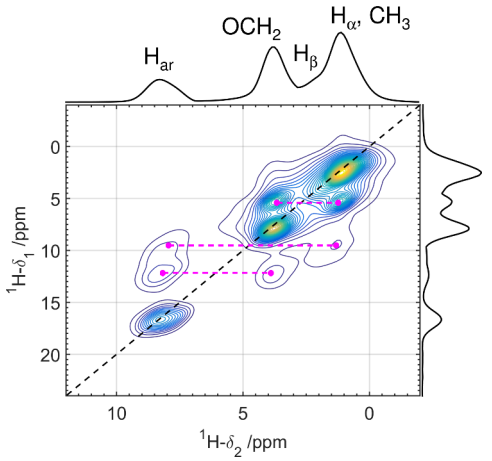

Figure 6. 2D ^{1}H DQ-SQ correlation spectrum for the NDI-silane crystal. The black dashed curve indicates the $2\delta-\delta$ DQ-SQ diagonal. Peak assignments are provided in the figure, and magenta dashed curves highlight relevant DQ-SQ correlations.

Again, the two peaks related to the ethoxysilane groups are due to the nonequivalent molecules in the unit cell.

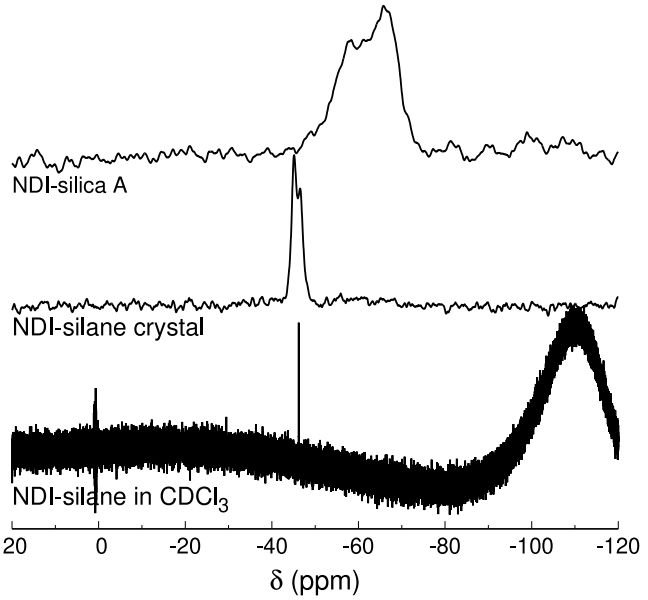

Figure 7. ^{29}Si NMR spectra of the NDI-silane in $CDCl_3$, the NDI-silane crystal and NDI-silica A. The ^{29}Si NMR spectrum of the NDI-silane in $CDCl_3$ shows a broad peak around −110 ppm, which belongs to the NMR tube.

3.3. Optical and Photoconductivity Characterization of NDI-silane Thin Films

In order to demonstrate the potential materials and properties that can be obtained from the NDI-silane crystals, we prepared NDI-silane as a thin film in the first approach. We characterized it concerning the optical properties and photoconductivity. It is important to remark that, when the precursor is obtained as stable and pure crystals, thin films could be prepared with controlled thickness and homogeneity from solutions with well-defined concentrations of the desired solvent (see section 2.2). Figure 8 shows the images and morphology of the thin films with better thicknesses after heat treatment from AFM images. It shows a homogeneous surface

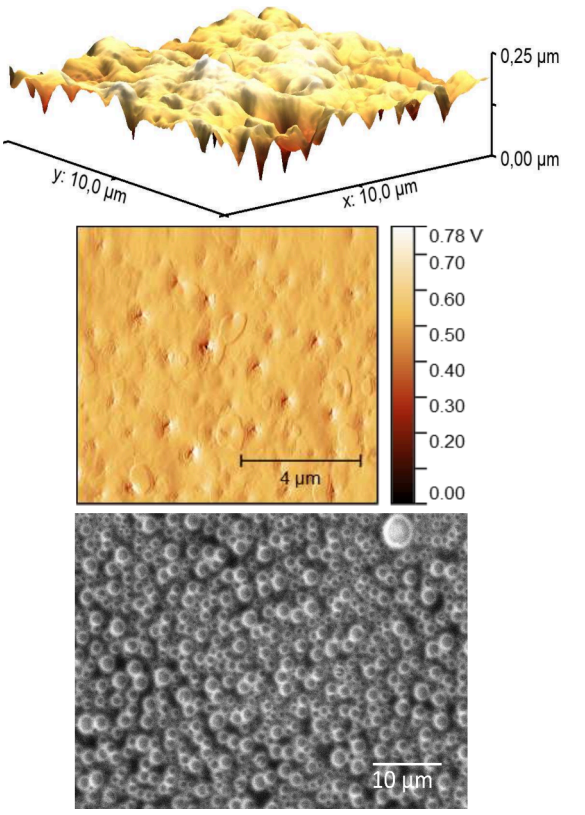

Figure 8. Topology and amplitude from the AFM (top) and SEM (bottom) images of the NDI-silane thin film.

with a roughness on a submicron scale and a film thickness of about 250 nm. This result could be reproducibly obtained from a THF solution with a concentration of 30 g/L, a droplet volume of 150 μL, and a rotation speed of 850 rpm for 30 s. The SEM image confirms that the molecules aggregate in a micrometric scale, interestingly, in a spherical shape.

Figure 9 shows the absorption and emission spectra obtained for the toluene solution and NDI-silane as the

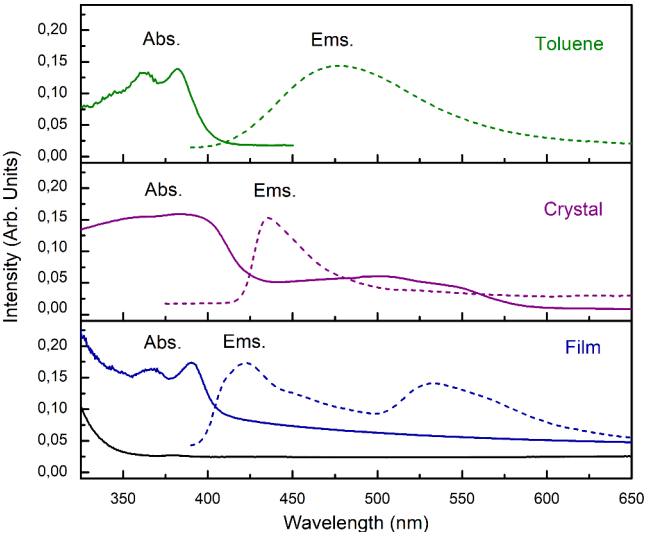

Figure 9. (Left) UV−vis absorption and (right) emission spectra with excitation at 365 nm for NDI-silane in a 10^{-4} M toluene solution, crystal, the thin film, and the glass substrate.

https://doi.org/10.1021/acsaenm.4c00341
ACS Appl. Eng. Mater. 2024, 2, 1976−1986

molecular crystal compared to a thin film and glass substrate. Absorption bands of NDI-silane in toluene are observed around 380 and 362 nm. In the crystal, there is a broad band from 425 nm extending to the UV, and in the thin film, it shows absorption bands around 390 and 370 nm, both slightly red-shifted in comparison to the toluene solution. The red-shifted absorption bands are associated with aggregates, either in the crystal or in the thin film. In order to confirm that, we calculated the first excited states for NDI-silane as an isolated molecule and for a cluster of four molecules as an H-aggregate system [see the DFT and TD-DFT calculation details in section 2.12, transitions listed in Table S3, and electron−hole natural transition orbitals (NTOs) in Figure S11].[35] We are considering here that the isolated molecule approximates to the molecule in toluene because it is an apolar and aprotic solvent. The cluster of molecule in the plane-to-plane configuration is one of the many viable molecular arrangements in the film. The isolated molecule shows a first optically excited state as S_2 at 3.64 eV (340 nm) with an oscillator strength (O.S.) of 0.16. The cluster system shows the first optically active state as S_{20} at 3.42 eV (362 nm) and an O.S. of 0.10, slightly red-shifted concerning the isolated molecule.

The emission spectra of NDI-silane in a toluene solution show a broad band around 470 nm, similar to organosilica in diluted concentrations,[6] attributed to the lowest excited-state decay of the monomer. Differently, the NDI-silane crystals show an emission around 430 nm, and the film shows well-defined emission bands around 420 and 540 nm upon excitation at 365 nm. As expected, the red-shifted absorption bands and the splitting of the emission band into the crystals and thin film compared to the diluted solution are related to aggregates. The two emission peaks are associated with the decay of the lowest excited electronic states of NDI-silane as H-like aggregates (420 nm), present in the crystal structure and film, and J-like aggregates (540 nm), present only in the film.[64]

Figure 10 shows the resistance of the NDI-silane film in the dark compared to the film irradiated with a 405 nm laser as a function of temperature in the range of 10−300 K. As expected, in both cases, the resistance decays as the temperature increases. This is the typical behavior of an intrinsic semiconductor and is related to the rise in energy available to promote charge carriers between bands and the generation of free charges as temperature increases. The NDI-silane film showed high resistances in the dark, going from 5000 MΩ at room temperature to 25000 MΩ at 10 K. When light shines on the sample, the resistances decrease abruptly to about 10 MΩ at room temperature, going to 25 MΩ at 10 K. The photoresistance observed is quite low for organic semiconductors. For instance, a blend of MEH-PPV (90 wt %) with C70 (10 wt %), which is a donor−acceptor polymeric system optimized as a device, shows a corresponding resistance of about 25 MΩ/mm at room temperature.[65] Note that the S_1 NTO hole of the cluster system is localized in one specific molecule, while the electron NTO is displaced over a second coupled molecule (Figure S11).[35] Thus, the conductivity enhancement under laser exposure is related to the photo-induced charge delocalization of the NDIs coupled as aggregates.

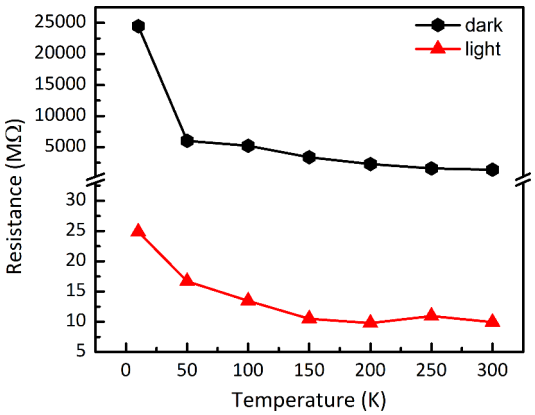

Figure 10. Resistance as a function of the temperature of the NDI-silane thin film in the dark and under λ = 405 nm laser irradiation.

3.4. Mesoporous NDI-silica

Mesoporous organosilica were prepared with NDI-silane via the sol−gel route in an acetone/ethanol solution in the presence of the IL 1-butyl-3methylimidazolium tetrafluoroborate. In this synthetic route, the IL acts as a mesoporous templating and sol−gel catalytic agent.[66] The materials were prepared from precursor solutions with NDI-silane:IL molar ratios of 1:2, 2:1, and 4:1, labeled as NDI-silica A, B, and C, respectively (Table 1).

Figures 4 and 7 also show the ^{13}C and ^{29}Si NMR spectra of NDI-silica A as representative spectra of the mesoporous materials. The ^{13}C CP-MAS NMR spectrum of NDI-silica A shows the same peaks as the NDI-silane crystal, except for the absence of the peaks at 58.4 and 18.3 ppm, belonging to the ethyl groups that should disappear after sol−gel hydrolysis and condensation (Figure 4, left). It also observed some additional broadening due to the amorphous nature of the silica network. Additionally, the $^{1}H\{^{13}C\}$ HETCOR spectrum for NDI-silica, shown in Figure S9,[35] shows the expected intramolecular correlations, confirming the integrity of the NDI organic moieties after the sol−gel reactions. The ^{29}Si NMR spectrum shows two peaks at −59 and −66 ppm coming from the T^2 and T^3 siloxane groups,[67] with contributions of 66% and 34%, respectively (Figure 7). The absence of ethyl carbons and only siloxane T_2 and T_3 groups indicate the complete hydrolyzation and high condensation of the sol−gel reaction with some remaining siloxyl groups.

Figure 11 also shows the TGA plot of NDI-silica A in contrast to that of the NDI-silane crystal. The NDI-silane

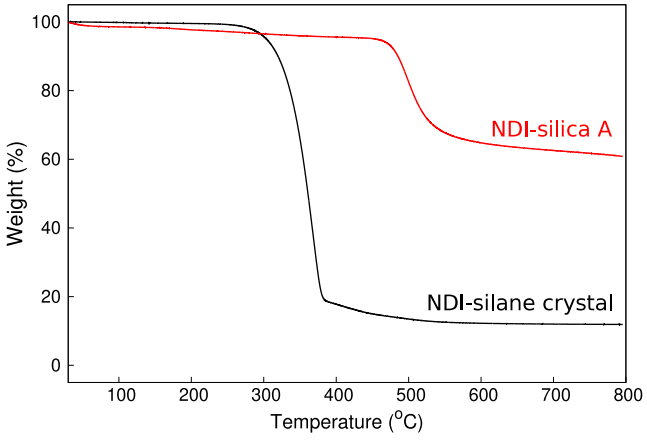

Figure 11. TGA plots of the NDI-silane crystal and NDI-silica A.

https://doi.org/10.1021/acsaenm.4c00341
ACS Appl. Eng. Mater. 2024, 2, 1976−1986

crystal shows an onset decomposition at 290 °C, similar to other NDI derivatives.[68,69] Interestingly, there is no weight loss due to adsorbed water, although the measurement was done without previous thermal treatment, indicating absent structural water or adsorbed in the crystals. The mesoporous material shows an onset of decomposition at 460 °C, significantly higher than that of the NDI-silane crystal, demonstrating that the silica network contributes to the thermal stability of the material.

Figure 12 shows the N_2 adsorption of NDI-silica A, B, and C, with their respective BJH pore size distributions.[70] The pore

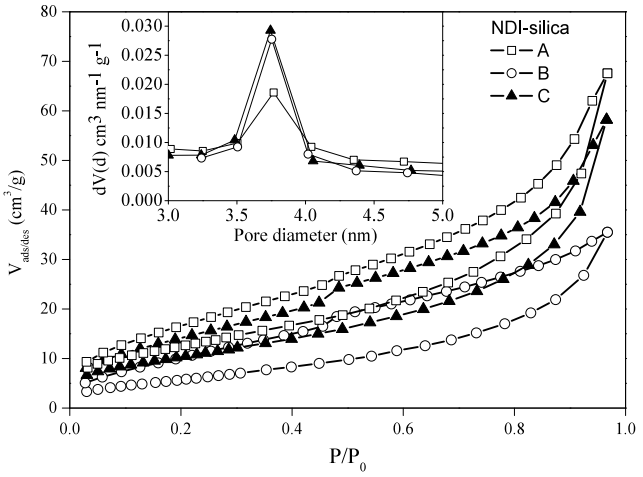

Figure 12. N_2 adsorption isotherms of NDI-silica A, B, and C, with their respective BJH pore diameter distributions.[70]

diameters are about 3.8 ± 0.3 nm wide, classified as mesoporous materials.[71] The BET surface areas[47] are given by 45.9, 22.0, and 38.0 m^2/g for NDI-silica A, B, and C, respectively. The isotherms resemble the H3 or H4 type,[71] associated with narrow slitlike pores. They also show pronounced hysteresis at low relative pressure, indicating irreversible uptake of molecules in pores or irreversible chemical interaction between N_2 and NDI groups. Figure 13 shows the TEM images of the mesoporous NDI-silica. We observe some control in morphology by using different NDI-silane/IL ratios. NDI-silica A is observed mostly as fibers in the micrometric scale, NDI-silica B is more spherical, and NDI-silica C is spherical with a systematic presence of a nucleus, indicating the presence of a more dense organosilica network. In agreement with the interpretation of the N_2 isotherms, one cannot observe nanopores in the scale of large pores, >10 nm, but there is some contrast/rugosity in the nanometer scale (right panels of Figure 13).

Thus, these materials demonstrate attractive alternatives for active hosting materials, such as donor–acceptor molecular systems for photoinduced charge separation. We are currently exploring this organosilica backbone to propose durable organic photovoltaic systems.

4. CONCLUSIONS

We have obtained *N,N′*-bis[3-(triethoxysilyl)propyl]-1,4,5,8-naphthalenediimide as stable molecular crystals and characterized its structure by combining experimental and theoretical techniques. We obtained the crystallographic structure using SCXRD and used this information to index by TEM, electron diffraction, and PXRD. Because ethoxysilane is a highly

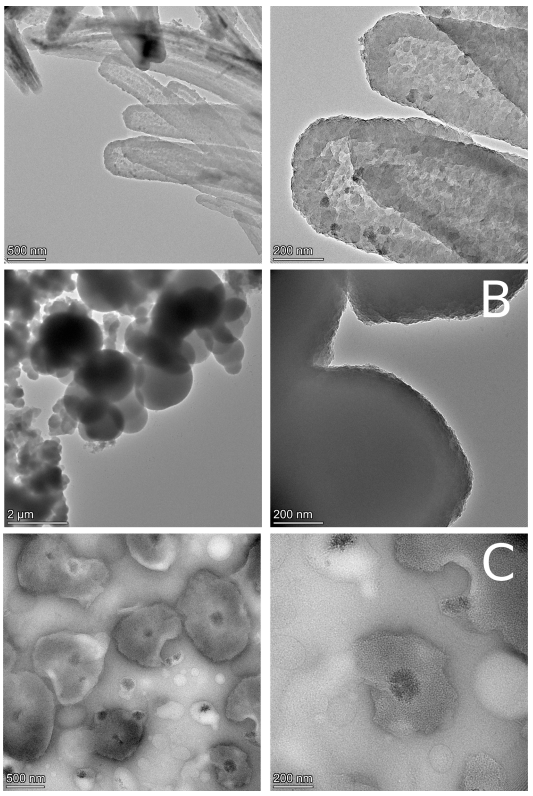

Figure 13. TEM images of NDI-silica A, B, and C.

reactive sol–gel group in the presence of water, the crystal stability is rationalized based on the intermolecular interactions. This represents a significant advance in the preparation of naphthalenediimide organosilica because it allows for the combination of the electronic properties of naphthalenediimide with the silica backbone in a highly flexible manner. This opens up new possibilities for the development of inorganic–organic electronic devices with high durability. As a proof of concept, we prepared NDI-silane thin films and mesoporous materials using 1-butyl-3methylimidazolium tetrafluoroborate as a templating and sol–gel catalytic agent. The films demonstrate a remarkable decrease in electrical resistance under laser illumination. The mesoporous materials demonstrate reasonable surface areas of about 40 m^2/g and narrow slitlike pores of about 4 nm, indicating irreversible uptake properties. Thus, these materials are promising candidates to structure devices with stable photoinduced charge-transfer mechanisms.

■ ASSOCIATED CONTENT

Supporting Information

The Supporting Information is available free of charge at https://pubs.acs.org/doi/10.1021/acsaenm.4c00341.

Crystal photographs, SCXRD, PXRD, and NMR data, TEM data, excited-state calculated data, and NTO plots (PDF)

■ AUTHOR INFORMATION

Corresponding Authors

Sergio Brochsztain − *Centro de Engenharia, Modelagem e Ciências Sociais Aplicadas, Universidade Federal do ABC, 09510-580 Santo André, São Paulo, Brazil;* orcid.org/

https://doi.org/10.1021/acsaenm.4c00341
ACS Appl. Eng. Mater. 2024, 2, 1976−1986

0000-0002-1129-8039; Email: sergio.brochsztain@ufabc.edu.br

Thiago Branquinho de Queiroz − *Centro de Ciências Naturais e Humanas, Universidade Federal do ABC, 09510-580 Santo André, São Paulo, Brazil;* orcid.org/0000-0003-3775-954X; Email: thiago.branquinho@ufabc.edu.br

Authors

Renan Gabriel de Assis − *Centro de Ciências Naturais e Humanas, Universidade Federal do ABC, 09510-580 Santo André, São Paulo, Brazil;* orcid.org/0000-0001-5992-0950

Marcos de Oliveira Junior − *Instituto de Física de São Carlos, Universidade de São Paulo, 13560-970 São Carlos, São Paulo, Brazil;* orcid.org/0000-0001-6538-2204

Márcia Tsuyama Escote − *Centro de Engenharia, Modelagem e Ciências Sociais Aplicadas, Universidade Federal do ABC, 09510-580 Santo André, São Paulo, Brazil;* orcid.org/0000-0003-1053-560X

Carlos Basílio Pinheiro − *Laboratório de Cristalografia, Departamento de Física, Universidade Federal de Minas Gerais, 31270-901 Belo Horizonte, Minas Gerais, Brazil;* orcid.org/0000-0002-8674-1779

José Javier Sáez Acuña − *Centro de Ciências Naturais e Humanas, Universidade Federal do ABC, 09510-580 Santo André, São Paulo, Brazil;* orcid.org/0009-0005-1026-6755

Fabio Furlan Ferreira − *Centro de Ciências Naturais e Humanas, Universidade Federal do ABC, 09510-580 Santo André, São Paulo, Brazil;* orcid.org/0000-0003-1516-1221

Luana Sucupira Pedroza − *Instituto de Física, Universidade de São Paulo, 0558-090 São Paulo, São Paulo, Brazil;* orcid.org/0000-0003-1454-1919

Complete contact information is available at: https://pubs.acs.org/10.1021/acsaenm.4c00341

Funding

The Article Processing Charge for the publication of this research was funded by the Coordination for the Improvement of Higher Education Personnel - CAPES (ROR identifier: 00x0ma614).

Notes

The authors declare no competing financial interest.

■ ACKNOWLEDGMENTS

The authors acknowledge the support of FAPESP (Grants 2020/13466-1, 2023/01502-1, 2017/10292-0, 2021/07694-4, 2022/02974-1, 2023/08771-8, and 2013/07793-6), CNPq (Grants 405048/2021-1 and 311069/2020-7), and ANP-PRN. The authors are grateful to the multiuser central facilities UFABC-ProPes for experimental support.

■ REFERENCES

(1) Kumar, S.; Shukla, J.; Kumar, Y.; Mukhopadhyay, P. Electron-poor arylenediimides. *Org. Chem. Front.* **2018**, *5*, 2254−2276.

(2) Chen, Z.; Zheng, Y.; Yan, H.; Facchetti, A. Naphthalenedicarboximide- vs Perylenedicarboximide-Based Copolymers. Synthesis and Semiconducting Properties in Bottom-Gate N-Channel Organic Transistors. *J. Am. Chem. Soc.* **2009**, *131*, 8−9.

(3) Bhosale, S. V.; Al Kobaisi, M.; Jadhav, R. W.; Morajkar, P. P.; Jones, L. A.; George, S. Naphthalene diimides: perspectives and promise. *Chem. Soc. Rev.* **2021**, *50*, 9845−9998.

(4) Hobson, S. T.; Shea, K. J. Bridged Bisimide Polysilsesquioxane Xerogels: New Hybrid Organic-Inorganic Materials. *Chem. Mater.* **1997**, *9*, 616−623.

(5) Croissant, J. G.; Cattoën, X.; Durand, J.-O.; Wong Chi Man, M.; Khashab, N. M. Organosilica hybrid nanomaterials with a high organic content: syntheses and applications of silsesquioxanes. *Nanoscale* **2016**, *8*, 19945−19972.

(6) Castanheira, B.; Triboni, E. R.; Andrade, L. d. S.; Trindade, F. d. J.; Otubo, L.; Teixeira, A. C. S. C.; Politi, M. J.; de Queiroz, T. B.; Brochsztain, S. Synthesis of Novel Periodic Mesoporous Organosilicas Containing 1,4,5,8-Naphthalenediimides within the Pore Walls and Their Reduction To Generate Wall-Embedded Free Radicals. *Langmuir* **2018**, *34*, 8195−8204.

(7) Mulfort, K. L.; Hupp, J. T. Chemical Reduction of Metal-Organic Framework Materials as a Method to Enhance Gas Uptake and Binding. *J. Am. Chem. Soc.* **2007**, *129*, 9604−9605.

(8) Shirman, E.; Ustinov, A.; Ben-Shitrit, N.; Weissman, H.; Iron, M. A.; Cohen, R.; Rybtchinski, B. Stable Aromatic Dianion in Water. *J. Phys. Chem. B* **2008**, *112*, 8855−8858.

(9) de Oliveira Marcon, R.; Bonvent, J.-J.; Brochsztain, S. Stabilization of free radicals in layer-by-layer nanoarchitectures containing multiple arylenediimides. *Dyes Pigm.* **2022**, *198*, 109948.

(10) Gosztola, D.; Niemczyk, M. P.; Svec, W.; Lukas, A. S.; Wasielewski, M. R. Excited Doublet States of Electrochemically Generated Aromatic Imide and Diimide Radical Anions. *J. Phys. Chem. A* **2000**, *104*, 6545−6551.

(11) Fujitsuka, M.; Kim, S. S.; Lu, C.; Tojo, S.; Majima, T. Intermolecular and Intramolecular Electron Transfer Processes from Excited Naphthalene Diimide Radical Anions. *J. Phys. Chem. B* **2015**, *119*, 7275−7282.

(12) Katz, H. E.; Lovinger, A. J.; Johnson, J.; Kloc, C.; Siegrist, T.; Li, W.; Lin, Y.-Y.; Dodabalapur, A. A soluble and air-stable organic semiconductor with high electron mobility. *Nature* **2000**, *404*, 478−481.

(13) Zhan, X.; Facchetti, A.; Barlow, S.; Marks, T. J.; Ratner, M. A.; Wasielewski, M. R.; Marder, S. R. Rylene and Related Diimides for Organic Electronics. *Adv. Mater.* **2011**, *23*, 268−284.

(14) Schmidt, G. C.; Höft, D.; Haase, K.; Hübler, A. C.; Karpov, E.; Tkachov, R.; Stamm, M.; Kiriy, A.; Haidu, F.; Zahn, D. R. T.; Yan, H.; Facchetti, A. Naphthalenediimide-based donor-acceptor copolymer prepared by chain-growth catalyst-transfer polycondensation: evaluation of electron-transporting properties and application in printed polymer transistors. *J. Mater. Chem. C* **2014**, *2*, 5149−5154.

(15) Han, Y.; Liu, Y.; Yuan, J.; Dong, H.; Li, Y.; Ma, W.; Lee, S.-T.; Sun, B. Naphthalene Diimide-Based n-Type Polymers: Efficient Rear Interlayers for High-Performance Silicon−Organic Heterojunction Solar Cells. *ACS Nano* **2017**, *11*, 7215−7222.

(16) Shukla, D.; Nelson, S. F.; Freeman, D. C.; Rajeswaran, M.; Ahearn, W. G.; Meyer, D. M.; Carey, J. T. Thin-Film Morphology Control in Naphthalene-Diimide-Based Semiconductors: High Mobility n-Type Semiconductor for Organic Thin-Film Transistors. *Chem. Mater.* **2008**, *20*, 7486−7491.

(17) Chen, Z.; Zheng, Y.; Yan, H.; Facchetti, A. Naphthalenedicarboximide- vs Perylenedicarboximide-Based Copolymers. Synthesis and Semiconducting Properties in Bottom-Gate N-Channel Organic Transistors. *J. Am. Chem. Soc.* **2009**, *131*, 8−9.

(18) Oh, J. H.; Suraru, S.; Lee, W.-Y.; Könemann, M.; Höffken, H. W.; Röger, C.; Schmidt, R.; Chung, Y.; Chen, W.-C.; Würthner, F.; Bao, Z. High-Performance Air-Stable n-Type Organic Transistors Based on Core-Chlorinated Naphthalene Tetracarboxylic Diimides. *Adv. Funct. Mater.* **2010**, *20*, 2148−2156.

(19) Rozanski, L. J.; Castaldelli, E.; Sam, F. L. M.; Mills, C. A.; Jean-François Demets, G.; Silva, S. R. P. Solution processed naphthalene diimide derivative as electron transport layers for enhanced brightness and efficient polymer light emitting diodes. *J. Mater. Chem. C* **2013**, *1*, 3347−3352.

(20) Wade, C. R.; Li, M.; Dincă, M. Facile Deposition of Multicolored Electrochromic Metal−Organic Framework Thin Films. *Angew. Chem., Int. Ed.* **2013**, *52*, 13377−13381.
(21) Xie, Y.-X.; Zhao, W.-N.; Li, G.-C.; Liu, P.-F.; Han, L. A Naphthalenediimide-Based Metal−Organic Framework and Thin Film Exhibiting Photochromic and Electrochromic Properties. *Inorg. Chem.* **2016**, *55*, 549−551.
(22) Garai, B.; Mallick, A.; Banerjee, R. Photochromic metal−organic frameworks for inkless and erasable printing. *Chem. Sci.* **2016**, *7*, 2195−2200.
(23) Liao, J.-Z.; Zhang, H.-L.; Wang, S.-S.; Yong, J.-P.; Wu, X.-Y.; Yu, R.; Lu, C.-Z. Multifunctional Radical-Doped Polyoxometalate-Based Host−Guest Material: Photochromism and Photocatalytic Activity. *Inorg. Chem.* **2015**, *54*, 4345−4350.
(24) Lyu, H.; Liu, J.; Mahurin, S.; Dai, S.; Guo, Z.; Sun, X.-G. Polythiophene coated aromatic polyimide enabled ultrafast and sustainable lithium ion batteries. *J. Mater. Chem. A* **2017**, *5*, 24083−24090.
(25) Pfeifer, S.; Schwarzer, A.; Schmidt, D.; Brendler, E.; Veith, M.; Kroke, E. Precursors for pyromellit-bridged silica sol−gel hybrid materials. *New J. Chem.* **2013**, *37*, 169−180.
(26) Pfeifer, S.; Brendler, E.; Veith, M.; Kroke, E. Hybrid-coatings derived from pyromellitic acid bridged alkoxy-silylalkyl precursors. *J. Sol-Gel Sci. Technol.* **2014**, *70*, 191−202.
(27) Schramm, C.; Rinderer, B.; Tessadri, R. Ladder-Like Aromatic Imide-Functionalized Poly(silsesquioxane): Preparation and Characterization via the Sol−Gel Route. *Advances in Polymer Technology* **2017**, *36*, 77−85.
(28) dos Santos Andrade, L.; Otubo, L.; Castanheira, B.; Brochsztain, S. Novel periodic mesoporous organosilicas containing pyromellitimides and their application for the photodegradation of asphaltenes. *Microporous Mesoporous Mater.* **2021**, *312*, 110740.
(29) Luo, Y.; Lin, J.; Duan, H.; Zhang, J.; Lin, C. Self-directed Assembly of Photoactive Perylenediimide-Bridged Silsesquioxane into a Superlong Tubular Structure. *Chem. Mater.* **2005**, *17*, 2234−2236.
(30) Ribeiro, T.; Baleizão, C.; Farinha, J. P. S. Synthesis and Characterization of Perylenediimide Labeled Core-Shell Hybrid Silica-Polymer Nanoparticles. *J. Phys. Chem. C* **2009**, *113*, 18082−18090.
(31) Wahab, M. A.; Hussain, H.; He, C. Photoactive Perylenediimide-Bridged Silsesquioxane Functionalized Periodic Mesoporous Organosilica Thin Films (PMO-SBA15): Synthesis, Self-Assembly, and Photoluminescent and Enhanced Mechanical Properties. *Langmuir* **2009**, *25*, 4743−4750.
(32) Wang, H.; Schaefer, K.; Pich, A.; Moeller, M. Synthesis of Silica Encapsulated Perylenetetracarboxylic Diimide Core−Shell Nanoellipsoids. *Chem. Mater.* **2011**, *23*, 4748−4755.
(33) Rathnayake, H.; Binion, J.; McKee, A.; Scardino, D. J.; Hammer, N. I. Perylenediimide functionalized bridged-siloxane nanoparticles for bulk heterojunction organic photovoltaics. *Nanoscale* **2012**, *4*, 4631−4640.
(34) Moraes, T. B.; Schimidt, M. F.; Bacani, R.; Weber, G.; Politi, M. J.; Castanheira, B.; Brochsztain, S.; Silva, F. de A.; Demets, G. J.-F.; Triboni, E. R. Polysilsesquioxane naphthalenediimide thermo and photochromic gels. *J. Lumin.* **2018**, *204*, 685−691.
(35) See the Supporting Information for NMR data.
(36) de Queiroz, T. B.; Botelho, M. B. S.; De Boni, L.; Eckert, H.; de Camargo, A. S. S. Strategies for reducing dye aggregation in luminescent host-guest systems: Rhodamine 6G incorporated in new mesoporous sol-gel hosts. *J. Appl. Phys.* **2013**, *113*, 113508.
(37) Clark, R. C.; Reid, J. S. The analytical calculation of absorption in multifaceted crystals. *Acta Crystallogr., Sect. A* **1995**, *51*, 887−897.
(38) Sheldrick, G. M. A short history of *SHELX*. *Acta Crystallogr., Sect. A* **2008**, *64*, 112−122.
(39) Sheldrick, G. M. *SHELXT* − Integrated space-group and crystal-structure determination. *Acta Crystallogr., Sect. A* **2015**, *71*, 3−8.
(40) Farrugia, L. J. *WinGX* and *ORTEP for Windows*: an update. *J. Appl. Crystallogr.* **2012**, *45*, 849−854.
(41) Sheldrick, G. M. Crystal structure refinement with *SHELXL*. *Acta Crystallographica Section C* **2015**, *71*, 3−8.
(42) Bennett, A. E.; Rienstra, C. M.; Auger, M.; Lakshmi, K. V.; Griffin, R. G. Heteronuclear decoupling in rotating solids. *J. Chem. Phys.* **1995**, *103*, 6951−6958.
(43) Mafra, L.; Siegel, R.; Fernandez, C.; Schneider, D.; Aussenac, F.; Rocha, J. High-resolution ^{1}H homonuclear dipolar recoupling NMR spectra of biological solids at MAS rates up to 67kHz. *J. Magn. Reson.* **2009**, *199*, 111−114.
(44) Wiench, J. W.; Bronnimann, C. E.; Lin, V. S.; Pruski, M. Chemical shift correlation NMR spectroscopy with indirect detection in fast rotating solids: Studies of organically functionalized mesoporous silicas. *J. Am. Chem. Soc.* **2007**, *129*, 12076−12077.
(45) Kimura, H.; Nakamura, K.; Eguchi, A.; Sugisawa, H.; Deguchi, K.; Ebisawa, K.; Suzuki, E. I.; Shoji, A. Structural study of a-amino-acid crystals by 1H CRAMPS NMR spectroscopy. *J. Mol. Struct.* **1998**, *447*, 247−255.
(46) Potrzebowski, M.; Tekely, P.; Dusausoy, Y. Comment to 13C-NMR Studies of Alpha and Gamma Polymorphs of Glycine. *Solid State Nucl. Magn. Reson.* **1998**, *11*, 253−257.
(47) Brunauer, S.; Emmett, P. H.; Teller, E. Adsorption of Gases in Multimolecular Layers. *J. Am. Chem. Soc.* **1938**, *60*, 309−319.
(48) Barrett, E. P.; Joyner, L. G.; Halenda, P. P. The determination of pore volume and area distributions in porous substances. I. Computations from nitrogen isotherms. *Journal of the American Chemical society* **1951**, *73*, 373−380.
(49) García, A.; et al. Siesta: Recent developments and applications. *J. Chem. Phys.* **2020**, *152*, 204108.
(50) Berland, K.; Hyldgaard, P. Exchange functional that tests the robustness of the plasmon description of the van der Waals density functional. *Phys. Rev. B* **2014**, *89*, 035412.
(51) Troullier, N.; Martins, J. L. Efficient pseudopotentials for plane-wave calculations. *Phys. Rev. B* **1991**, *43*, 1993−2006.
(52) Zhao, Y.; Truhlar, D. G. The M06 suite of density functionals for main group thermochemistry, thermochemical kinetics, noncovalent interactions, excited states, and transition elements: two new functionals and systematic testing of four M06-class functionals and 12 other functionals. *Theor. Chem. Acc.* **2008**, *120*, 215−241.
(53) Boys, S.; Bernardi, F. The calculation of small molecular interactions by the differences of separate total energies. Some procedures with reduced errors. *Mol. Phys.* **1970**, *19*, 553−566.
(54) Yeh, M.-Y.; Lin, H.-C. Theoretical analysis of the intermolecular interactions in naphthalene diimide and pyrene complexes. *Phys. Chem. Chem. Phys.* **2014**, *16*, 24216−24222.
(55) Vydrov, O. A.; Scuseria, G. E. Assessment of a long-range corrected hybrid functional. *J. Chem. Phys.* **2006**, *125*, 234109.
(56) Stein, T.; Kronik, L.; Baer, R. Reliable prediction of charge transfer excitations in molecular complexes using time-dependent density functional theory. *J. Am. Chem. Soc.* **2009**, *131*, 2818−2820.
(57) Peach, M. J. G.; Benfield, P.; Helgaker, T.; Tozer, D. J. Excitation energies in density functional theory: an evaluation and a diagnostic test. *J. Chem. Phys.* **2008**, *128*, 044118.
(58) Niedzialek, D.; Duchemin, I.; de Queiroz, T. B.; Osella, S.; Rao, A.; Friend, R.; Blase, X.; Kümmel, S.; Beljonne, D. First Principles Calculations of Charge Transfer Excitations in Polymer-Fullerene Complexes: Influence of Excess Energy. *Adv. Funct. Mater.* **2015**, *25*, 1972−1984.
(59) Shao, Y.; et al. Advances in methods and algorithms in a modern quantum chemistry program package. *Phys. Chem. Chem. Phys.* **2006**, *8*, 3172−3191.
(60) Schaftenaar, G.; Noordik, J. J. Molden: a pre- and post-processing program for molecular and electronic structures. *J. Comput.-Aided Mol. Design* **2000**, *14*, 123−134.
(61) Humphrey, W.; Dalke, A.; Schulten, K. VMD − Visual Molecular Dynamics. *J. Mol. Graphics* **1996**, *14*, 33−38.
(62) Wang, F.; Nimmo, S. L.; Cao, B.; Mao, C. Oxide formation on biological nanostructures via a structure-directing agent: towards an understanding of precise structural transcription. *Chem. Sci.* **2012**, *3*, 2639−2645.

https://doi.org/10.1021/acsaenm.4c00341
ACS Appl. Eng. Mater. 2024, 2, 1976−1986

(63) Kumar, N. S. S.; Gujrati, M. D.; Wilson, J. N. Evidence of preferential π-stacking: a study of intermolecular and intramolecular charge transfer complexes. *Chem. Commun.* **2010**, *46*, 5464−5466.
(64) Kasha, M.; Rawls, H. R.; El-Bayoumi, M. A. The exciton model in molecular spectroscopy. *Pure Appl. Chem.* **1965**, *11*, 371.
(65) Yakuphanoglu, F. Electrical conductivity, optical and metal-semiconductor contact properties of organic semiconductor based on MEH-PPV/fullerene blend. *J. Phys. Chem. Solids* **2008**, *69*, 949−954.
(66) Karout, A.; Pierre, A. C. Silica gelation catalysis by ionic liquids. *Catal. Commun.* **2009**, *10*, 359−361.
(67) Jitianu, A.; Cadars, S.; Zhang, F.; Rodriguez, G.; Picard, Q.; Aparicio, M.; Mosa, J.; Klein, L. C. 29Si NMR and SAXS investigation of the hybrid organic-inorganic glasses obtained by consolidation of the melting gels. *Dalton Trans.* **2017**, *46*, 3729−3741.
(68) Li, J.; Hu, Y.-H.; Ge, C.-W.; Gong, H.-G.; Gao, X.-K. The role of halogen bonding in improving OFET performance of a naphthalenediimide derivative. *Chin. Chem. Lett.* **2018**, *29*, 423−428.
(69) Ali, S.; Jameel, M. A.; Gupta, A.; Langford, S. J.; Shafiei, M. Capacitive humidity sensing performance of naphthalene diimide derivatives at ambient temperature. *Synth. Met.* **2021**, *275*, 116739.
(70) Brunauer, S.; Emmett, P. H.; Teller, E. Adsorption of Gases in Multimolecular Layers. *J. Am. Chem. Soc.* **1938**, *60*, 309−319.
(71) Sing, K. S. W. Reporting physisorption data for gas/solid systems with special reference to the determination of surface area and porosity (Recommendations 1984). *Pure Appl. Chem.* **1985**, *57*, 603−619.

https://doi.org/10.1021/acsaenm.4c00341
ACS Appl. Eng. Mater. 2024, 2, 1976−1986